



OPEN ACCESS

EDITED BY

Stefan Liebau,
University of Tübingen, Germany

REVIEWED BY

Eric C. Olson,
Upstate Medical University,
United States
Monica Suarez Korsnes,
Norwegian University of Science and
Technology, Norway

*CORRESPONDENCE

Steven Finkbeiner,
steve.finkbeiner@gladstone.ucsf.edu

[†]These authors have contributed equally
to this work

SPECIALTY SECTION

This article was submitted to
Neurotoxicology,
a section of the journal
Frontiers in Toxicology

RECEIVED 03 May 2022

ACCEPTED 27 July 2022

PUBLISHED 24 August 2022

CITATION

Wang S, Linsley JW, Linsley DA,
Lamstein J and Finkbeiner S (2022),
Fluorescently labeled nuclear
morphology is highly informative
of neurotoxicity.
Front. Toxicol 4:935438.
doi: 10.3389/ftox.2022.935438

COPYRIGHT

© 2022 Wang, Linsley, Linsley, Lamstein
and Finkbeiner. This is an open-access
article distributed under the terms of the
[Creative Commons Attribution License
\(CC BY\)](https://creativecommons.org/licenses/by/4.0/). The use, distribution or
reproduction in other forums is
permitted, provided the original
author(s) and the copyright owner(s) are
credited and that the original
publication in this journal is cited, in
accordance with accepted academic
practice. No use, distribution or
reproduction is permitted which does
not comply with these terms.

Fluorescently labeled nuclear morphology is highly informative of neurotoxicity

Shijie Wang^{1†}, Jeremy W. Linsley^{1†}, Drew A. Linsley^{2,3†},
Josh Lamstein¹ and Steven Finkbeiner^{1,4,5,6,7*}

¹Center for Systems and Therapeutics, Gladstone Institutes, San Francisco, CA, United States, ²Robert J. and Nancy D. Carney Institute for Brain Science, Brown University, Providence, RI, United States, ³Department of Cognitive, Linguistic and Psychological Sciences, Brown University, Providence, RI, United States, ⁴Taube/Koret Center for Neurodegenerative Disease, Gladstone Institutes, San Francisco, CA, United States, ⁵Departments of Neurology and Physiology, University of California, San Francisco, San Francisco, CA, United States, ⁶Neuroscience Graduate Program, University of California, San Francisco, San Francisco, CA, United States, ⁷Biomedical Sciences Graduate Program, University of California, San Francisco, San Francisco, CA, United States

Neurotoxicity can be detected in live microscopy by morphological changes such as retraction of neurites, fragmentation, blebbing of the neuronal soma and ultimately the disappearance of fluorescently labeled neurons. However, quantification of these features is often difficult, low-throughput, and imprecise due to the overreliance on human curation. Recently, we showed that convolutional neural network (CNN) models can outperform human curators in the assessment of neuronal death from images of fluorescently labeled neurons, suggesting that there is information within the images that indicates toxicity but that is not apparent to the human eye. In particular, the CNN's decision strategy indicated that information within the nuclear region was essential for its superhuman performance. Here, we systematically tested this prediction by comparing images of fluorescent neuronal morphology from nuclear-localized fluorescent protein to those from freely diffused fluorescent protein for classifying neuronal death. We found that biomarker-optimized (BO-) CNNs could learn to classify neuronal death from fluorescent protein-localized nuclear morphology (mApple-NLS-CNN) alone, with super-human accuracy. Furthermore, leveraging methods from explainable artificial intelligence, we identified novel features within the nuclear-localized fluorescent protein signal that were indicative of neuronal death. Our findings suggest that the use of a nuclear morphology marker in live imaging combined with computational models such as mApple-NLS-CNN can provide an optimal readout of neuronal death, a common result of neurotoxicity.

KEYWORDS

cell death, microscopy, light, convolutional neural network, genetically encoded biosensor, live microscopy, neuronal death, excitotoxicity glutamatergic

Introduction

Neuronal death is frequently used to assess neurotoxicity *in vitro* (Kepp et al., 2011; Linsley et al., 2019a). A plethora of cell death indicators, dyes, and stains have been implemented to measure neuronal death in the assessment of neurotoxicity, yet application of these reagents in live microscopy can introduce artificial toxicity. Recently, we established a novel family of genetically encoded death indicators (GEDI) that acutely mark a stage at which neurons are irreversibly committed to die (Linsley et al., 2021a). The GEDI biosensor was engineered to signal only when intracellular Ca^{2+} reaches a level at which the cell has irreversibly committed to death, providing unparalleled accuracy and specificity. However, the GEDI approach has two main limitations. First, it requires that cells be transfected with the GEDI reporter, and second, the GEDI construct emits in two fluorescent channels, which limits the use of co-expressed biosensors.

To address these limitations we previously developed analysis techniques that are informed by GEDI biosensors to classify and quantify neuronal death using images of fluorescent neuronal morphology alone (Kim et al., 2014). Using convolutional neural networks (CNNs), we generated generalizable models that learned the signature of dead cells from a quantified label derived from the GEDI biosensor (Kim et al., 2014). Rather than generating large, labeled datasets of images through human curation and/or annotation, as is usually required for training CNNs (Hughes et al., 2018; Sullivan et al., 2018), we used quantification of the GEDI signal directly as a classification label, a technique we named biomarker-optimized convolutional neural networks (BO-CNNs). The resulting model showed superhuman accuracy at live/dead classification, and dramatic improvement in the speed of analysis.

Cell death is thought to occur when a cell has either lost membrane homeostasis or when the nucleus disintegrates (Galluzzi et al., 2009; Galluzzi et al., 2018). When membrane homeostasis is lost, a cell displays cytoplasmic shrinkage and plasma membrane blebbing and vacuolization, morphological alterations that are commonly used to classify cell death (Galluzzi et al., 2018). In contrast, labels that bind DNA upon disintegration of the nucleus and reflect chromatin condensation (pyknosis) or DNA fragmentation (karyorrhexis), such as DAPI or propidium iodide, often reflect a distinct signal from cell biology that can be used to classify the subroutine of cell death (Hou et al., 2016). By recording when extracellular Ca^{2+} has permeated into a cell to an irreversible level, the GEDI biosensor effectively reports loss of membrane homeostasis (Linsley et al., 2021a). Intriguingly, BO-CNNs trained to the GEDI biosensor appeared to use signal corresponding to the membrane and the nucleus to make live/dead classifications, despite the nuclear signal being difficult to distinguish by eye (Linsley et al., 2021b). This suggested that the nuclear morphology signal may actually be ideal for live/dead classification, perhaps by reflecting the collapse of the nuclear envelope. Nuclear morphology signal is often preferable to cell

morphology signal in live imaging experiments, particularly when tracking cells in dense cell culture or tissue (Hadjantonakis and Papaioannou, 2004; Kim et al., 2014; Tomer et al., 2015; Alladin et al., 2020), and the ability to detect death based on nuclear morphology could enable analysis of toxicity in these experiments as well.

Here, we compared the informativity of nuclear and morphology signals for indicating irreversible death by generating a novel BO-CNN trained to detect death in cells expressing nuclear-targeted mApple fluorescence (mApple-NLS-CNN). We found that after neuronal death, nuclear-localized fluorescent protein showed unique features from non-targeted mApple, and the mApple-NLS-CNN was better than humans at detecting death and rivaled the performance of BO-CNNs trained with non-targeted mApple (mApple-CNN). Nuclear-localized mApple (mApple-NLS) escaped from the nuclear envelope into the cytosol during death, filling out the neuronal morphology and highlighting membrane distortions. Relatedly, the mApple-NLS-CNN utilized a decision strategy to detect death distinct from that of the mApple-CNN: it focused on a previously unidentified, distinct, small punctate signal within the nucleus, a phenomenon associated with death that had not been previously described. These data suggest that nuclear morphology is a highly informative signal for identifying neuronal death and neurotoxicity.

Materials and methods

Primary neuron isolation and culture

Primary mouse neurons were prepared as previously described (Skibinski et al., 2017; Linsley et al., 2021a; Linsley et al., 2021b). In short, the cortex from prenatal mice at embryonic days 18–20 was dissected and dissociated in dissociation medium (DM) with kynurenic acid (1 mM final) (DM/KY) and treated with papain (100 U, Worthington Biochemical) and trypsin inhibitor solution (15 mg/ml trypsin inhibitor; Sigma). The cells were then gently resuspended into single neurons in Opti-MEM (Thermo Fisher Scientific) and glucose medium (20 mM), and were plated at 125,000 cells per well of a 96-well plate. Cells were maintained using a Neurobasal growth medium with 100 × GlutaMAX, B27 supplement (all from Gibco), and Pen/Strep. All animal experiments complied with the regulations of, and the protocol was approved by, the Institutional Animal Care Use Committee (IACUC) of the University of California, San Francisco (UCSF).

Plasmid transfection and staining

Mouse primary cortical neurons were transfected with 0.1 μg plasmids per well (96-well plate) and Lipofectamine 2000 on day

4 of culture. The plasmids hSyn-GC150-p2a-mApple and hSyn-GC150-3xNLS-p2a-mApple-3xNLS were previously described as a genetically encoded death indicator (GEDI) (Linsley et al., 2021a). Hoechst 33,342 Ready Flow™ Reagent (Thermo Fisher Scientific) was added to label DNA in live cell imaging.

Automated time-lapse imaging, image processing and quantification

Image processing and GEDI ratio quantification was previously described (Kim et al., 2014; Linsley et al., 2021a). To induce neuronal death, neurons were treated with 0.05 mM L-Glutamic acid monosodium salt diluted in NB media. Cells were imaged every 8 h after treatment using an automated time-lapse imaging system. The captured images were processed using custom-built scripts within a custom Galaxy bioinformatic cluster (Linsley et al., 2019b). In summary, the Galaxy bioinformatic cluster links image processing modules as a workflow, and can process image datasets in a batch. Image processing modules include background subtraction of the median intensity of each image, aligning images across longitudinal time points, segmenting individual neurons and tracking, extracting cell data including fluorescence intensity and cell size, and making crops for individual cells where the centroid of the cell is positioned at the center. To calculate the GEDI ratio, the mean intensity of the GEDI fluorescence signal (GC150 or GC150-NLS) was normalized to the morphological fluorescence signal (mApple or mApple-NLS). Live and dead cells were labeled in longitudinal imaging sets using empirically calculated GEDI thresholds. Crops for individual cells in the morphology channel were used for neural network model training. Precision-Recall curves were plotted using R. Group comparisons (t-test and paired t-test, Wilcoxon signed-rank test and ANOVA) were calculated in GraphPad Prism.

Training GEDI-CNNs

BO-CNNs were trained using PyTorch (https://github.com/drewlinsley/robo_ms_ai). Deep residual convolutional neural networks (ResNets), specifically the 18-layer ResNet, were used as the basic architecture in our experiments (He et al., 2015), which are the standard deep learning model for computer vision tasks like classification. Models were initialized with weights pre-trained on ImageNet and downloaded from the TorchVision library in Pytorch. Models were trained using batches of 32 images, a 1e-3 learning rate and the Adam optimizer for 200,000 steps of training (Kingma and Ba, 2014). In total, 6,778 images of either mApple or mApple-NLS transfected cells were used to train, validate, and test our models. In both cases, images were randomly allocated into non-overlapping sets for training (5,422 cells per group), validation

(678 cells per group), and testing (678 cells per group). The best-performing weights were selected according to the loss score measured on the validation set. All results reported in the manuscript reflect CNN performance on the testing set.

GEDI-CNN GradCAM

Guided GradCAM, which produces an interpretable map of the importance of visual features for a given image, was used in order to identify morphological features driving our models' decisions and was implemented through the Captum library (<https://captum.ai>) in PyTorch (Selvaraju et al., 2016). For the ResNet18, the denoising-gradient mask was computed at "layer two" of the model.

Curation tools

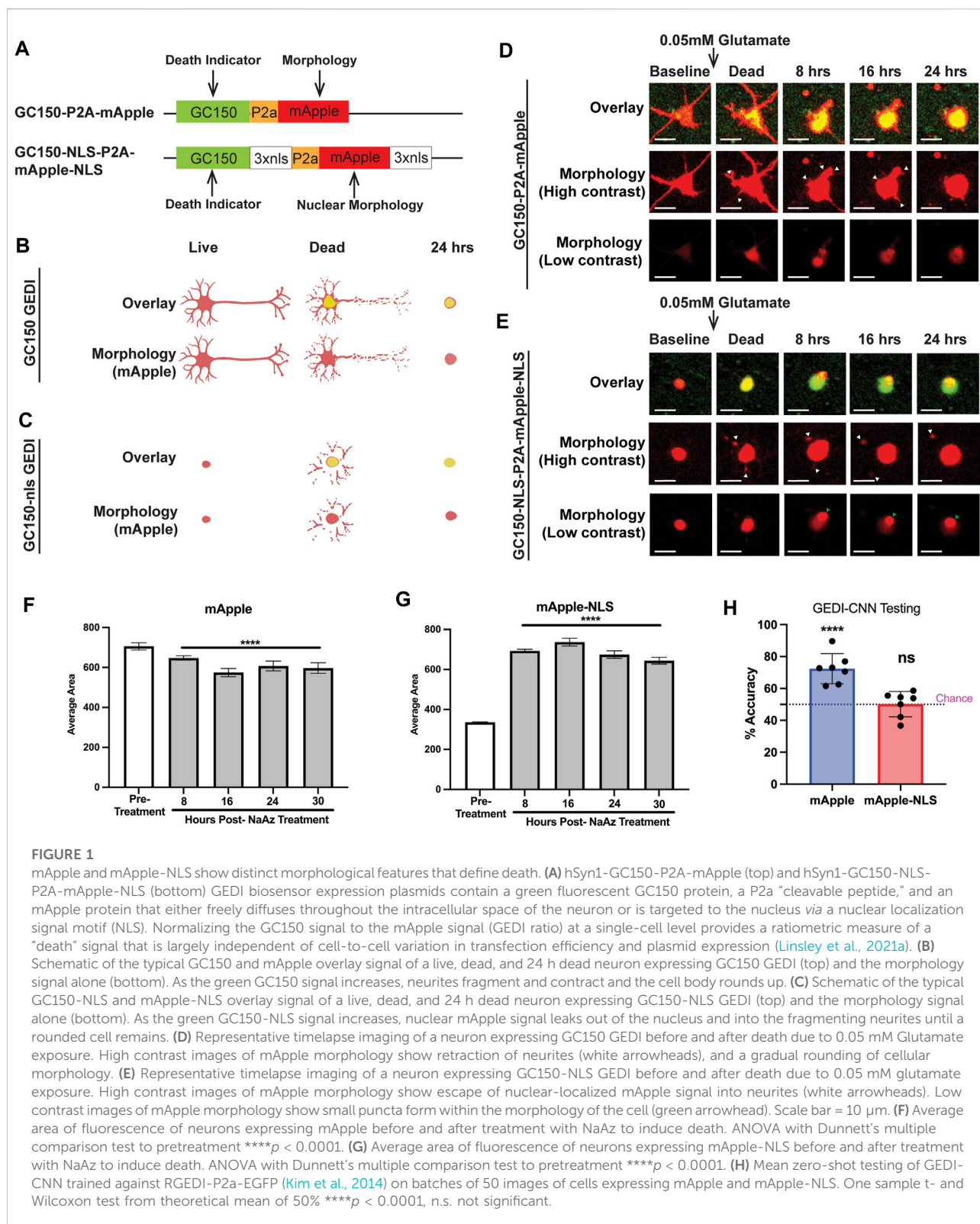
Curation was performed using a custom Fiji script that runs a graphical interface with a curator, displaying a blinded batch of cropped mApple or mApple-NLS morphology images one at a time while prompting the curator to indicate whether the displayed neuron is live or dead with a keystroke (ImageCurator.ijm).

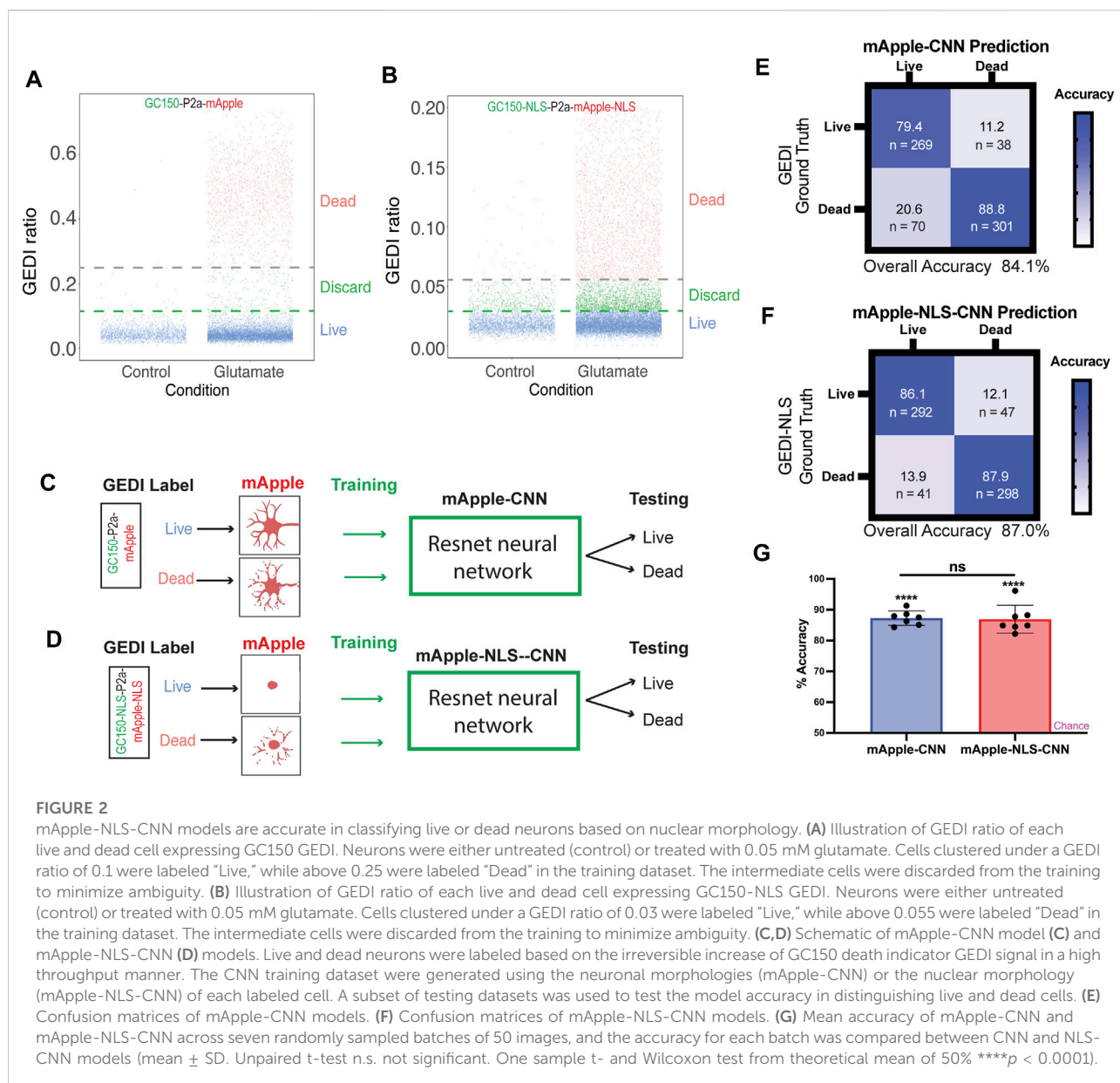
Results

Nuclear-localized fluorescent protein shows distinct features after death

In prior work, we used a genetically encoded death indicator (GEDI) as a supervision signal for a BO-CNN, training it to classify cell death from images of GFP-labeled cells. We named this instance of a BO-CNN the GEDI-CNN (Kim et al., 2014). The GEDI-CNN holds several advantages over the conventional GEDI biosensor, including that it only requires an EGFP morphology signal for use. Multiple GEDI biosensors have now been developed with different physiological properties and subcellular localizations. Here, we asked whether we could improve GEDI-CNN performance by using alternative GEDI biosensors, such as those with mApple rather than GFP as the fluorescent morphology indicator, with GC150 rather than RGEDI, which has a slightly higher Ca²⁺ binding affinity, as the death indicator, and with biosensors that were nuclear-targeted (Figures 1A–C).

To train GEDI-CNN models with different GEDI biosensors, primary rodent neurons were transfected with the non-targeted GC150-P2a-mApple or the nuclear-targeted GC150-NLS-P2a-mApple-NLS, exposed to 0.05 mM glutamate to trigger cell death, and longitudinally imaged over 24 h. Glutamate is the most common neurotransmitter in the brain, but excess





glutamate is toxic to neurons and the hypersensitivity of specific subsets of neurons to glutamate toxicity is associated with neurodegenerative disease (Zhou and Danbolt, 2014; Lewerenz and Maher, 2015). In both sets of transfected neurons, GC150 signal rapidly increased after glutamate exposure (Figures 1D,E). Morphological signals of neuronal degeneration have been well characterized (Cooper et al., 2017; Sherman and Bang, 2018; Linsley et al., 2019a). In GC150-P2a-mApple transfected neurons, the cytoplasmic mApple morphology signal recapitulated classical signs of degeneration after glutamate exposure, such as retraction of neurites and subsequent balling up of the soma (Figure 1D).

The changes in nuclear-localized fluorescence indicative of neurodegeneration have not been previously defined. Unexpectedly, we observed abrupt appearance of fragmented neurites in cells expressing mApple-NLS following glutamate treatment (Figure 1E; Supplementary Figure S1). Moreover, in contrast to the area of the non-targeted mApple signal, which gradually shrunk in size after cell death, the nuclear-localized mApple signal showed a significant enlargement of area after death (Figures 1D–G). Taken together, this suggests that upon cell death the mApple-NLS leaks out of the nuclear envelope and into the soma and neurites. Additionally, in many cases a small dense accumulation of mApple-NLS appeared after death (Figure 1E; Supplementary Movie S1) that was visible only

when the contrast of the image was set low, a phenomenon not previously reported.

To underscore the difference in features associated with death between mApple and mApple-NLS, we tested the GEDI-CNN model trained on EGFP neuronal morphology (Kim et al., 2014) on mApple and mApple-NLS images. The model translated well to images of non-targeted mApple, but scored no better than chance on images of nuclear-localized mApple (Figure 1H). These data suggest that mApple and nuclear-localized mApple each display distinct morphological features associated with neurodegeneration, and a CNN model trained with nuclear-localized mApple may be required to detect neuronal death using the nuclear-localized mApple signal.

BO-CNNs can be trained from GC150-P2a-mApple and GC150-NLS-P2a-mApple-NLS

As the morphological features associated with nuclear mApple are substantially different than those of cytoplasmic mApple, we next wondered how BO-CNNs trained on GC150-P2a-mApple and GC150-NLS-P2a-mApple-NLS datasets would compare. Large datasets were collected from GC150-P2a-mApple and GC150-NLS-P2a-mApple-NLS transfected neurons, and the GEDI ratios were plotted to classify live and dead neurons by their GEDI biosensor signal (Figures 2A,B). In total, 6,778 cropped mApple images and 6,778 cropped mApple-NLS images of neurons were sorted into live and dead categories with clear GEDI ratio cut-off, and intermediate signal buckets were not included in training the CNN model to avoid ambiguity, as described previously (Kim et al., 2014). Next, neural network models for mApple and mApple-NLS were trained with a ResNet architecture, and were evaluated for accuracy (Figures 2C–G). Both mApple-CNN and mApple-NLS showed significant accuracy on a balanced dataset with similar degrees of overall accuracy (Figure 2G). These data demonstrate that BO-CNN live/dead classifier models can be effectively trained on mApple and nuclear-mApple signals.

Live-dead BO-CNN developed with nuclear fluorescent protein shows superhuman accuracy

To test how well each model performs overall, we next compared their live/dead classification accuracy against that of human curators. Previously, we showed that GEDI-CNN models trained against EGFP morphology signal output live/dead classification with superhuman accuracy and speed (Kim et al., 2014). Similarly, the mApple-CNN achieved significantly higher accuracy than trained human curators, even with a much smaller training data set of mApple GEDI

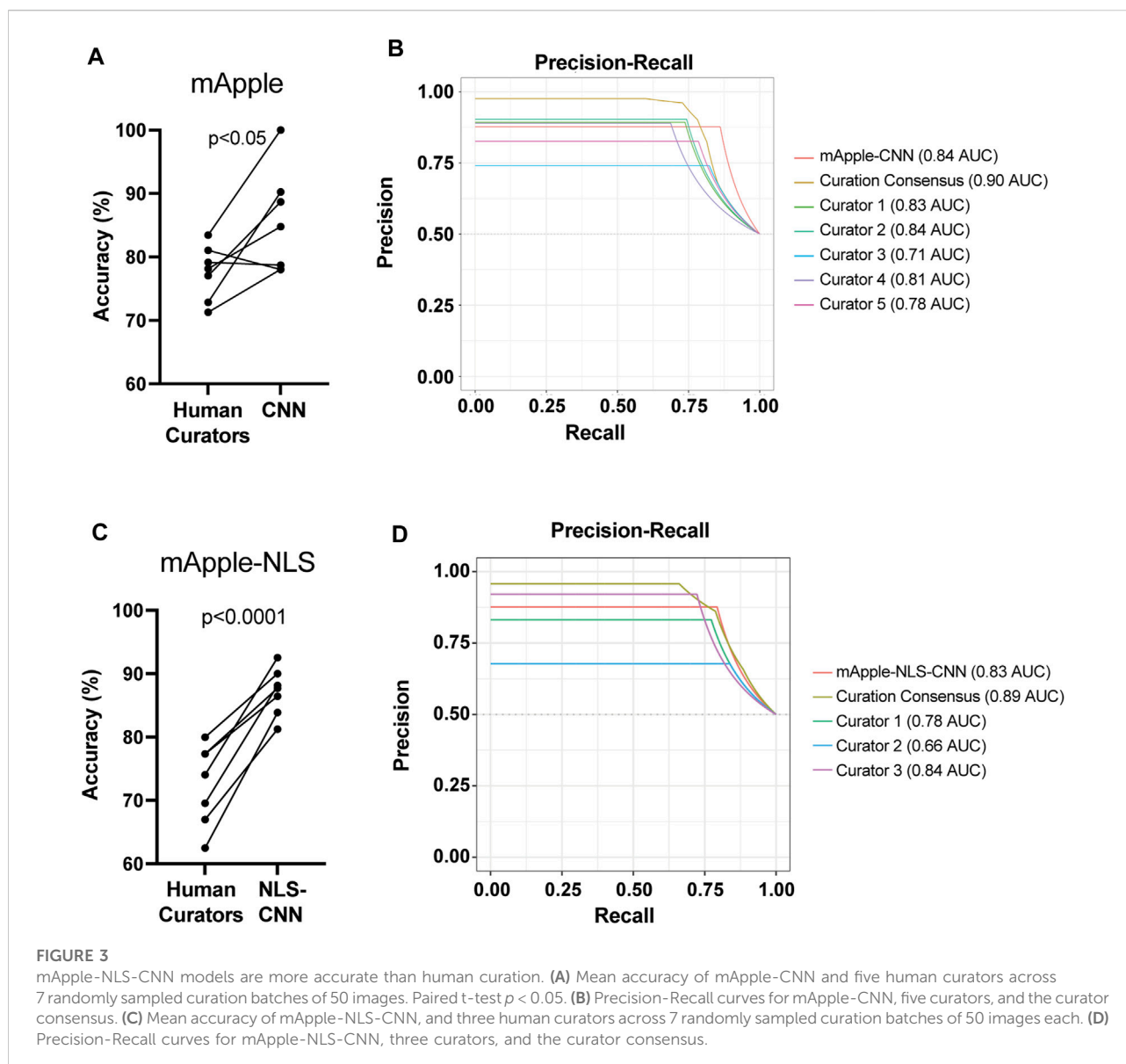
images (152,242 for GEDI-CNN vs. 8,132 for mApple-CNN) (Figures 3A,B). The mApple-NLS-CNN also performed with significantly better accuracy than human curators with the same smaller sized training set (Figures 3C,D). These data suggest BO-CNNs can be used to capture the unique morphological features marked by the nuclear-localized mApple signal.

mApple-NLS-CNN GradCAM highlights key features for classification of death in nuclear-mApple morphology

To explore which features of nuclear-localized mApple are most associated with neuronal death and with mApple-NLS-CNN classification accuracy, we used guided gradient-weighted class activation mapping (GradCAM), which we used previously to probe the decisions of the GEDI-CNN (Kim et al., 2014). GradCAM produces an interpretable map of the importance of visual features for a given image by deriving a gradient of the CNN's evidence for a selected class (i.e., dead) (Kim et al., 2014; Selvaraju et al., 2016). We generated GradCAM feature importance maps for both live and dead decisions for mApple-NLS-CNN, and compared them to the original mApple-NLS morphology images to map their localization. In examples of images correctly classified as live, the GradCAM signal typically lined the nuclear membrane (Figures 4A,C). In contrast, in examples correctly classified as dead, the GradCAM signal typically localized to either the dense accumulation of mApple signal visible when the image contrast was low or to fragmented neurites visible when the image contrast was set to high (Figures 4B,C). To identify the source and localization of the accumulated mApple signal, we performed a time-lapse experiment with GC150-NLS-P2a-mApple-NLS transfected neurons live stained with Hoechst 33,342 dye, a membrane permeable dye that binds DNA. Patterns of Hoechst 33,342 dye also change when cells die reflecting nuclear condensation, and have also been used to analyze cell death (Supplementary Figure S2) (Crowley et al., 2016). Dense mApple accumulations co-stained with Hoechst 33,342, indicating the mApple accumulations coincide with DNA condensation that occurs during apoptotic cell death (Toné et al., 2007) (Figure 4D). These data suggest that mApple-NLS-CNN recognizes unique features of nuclear-localized mApple to generate live/dead classifications.

Discussion

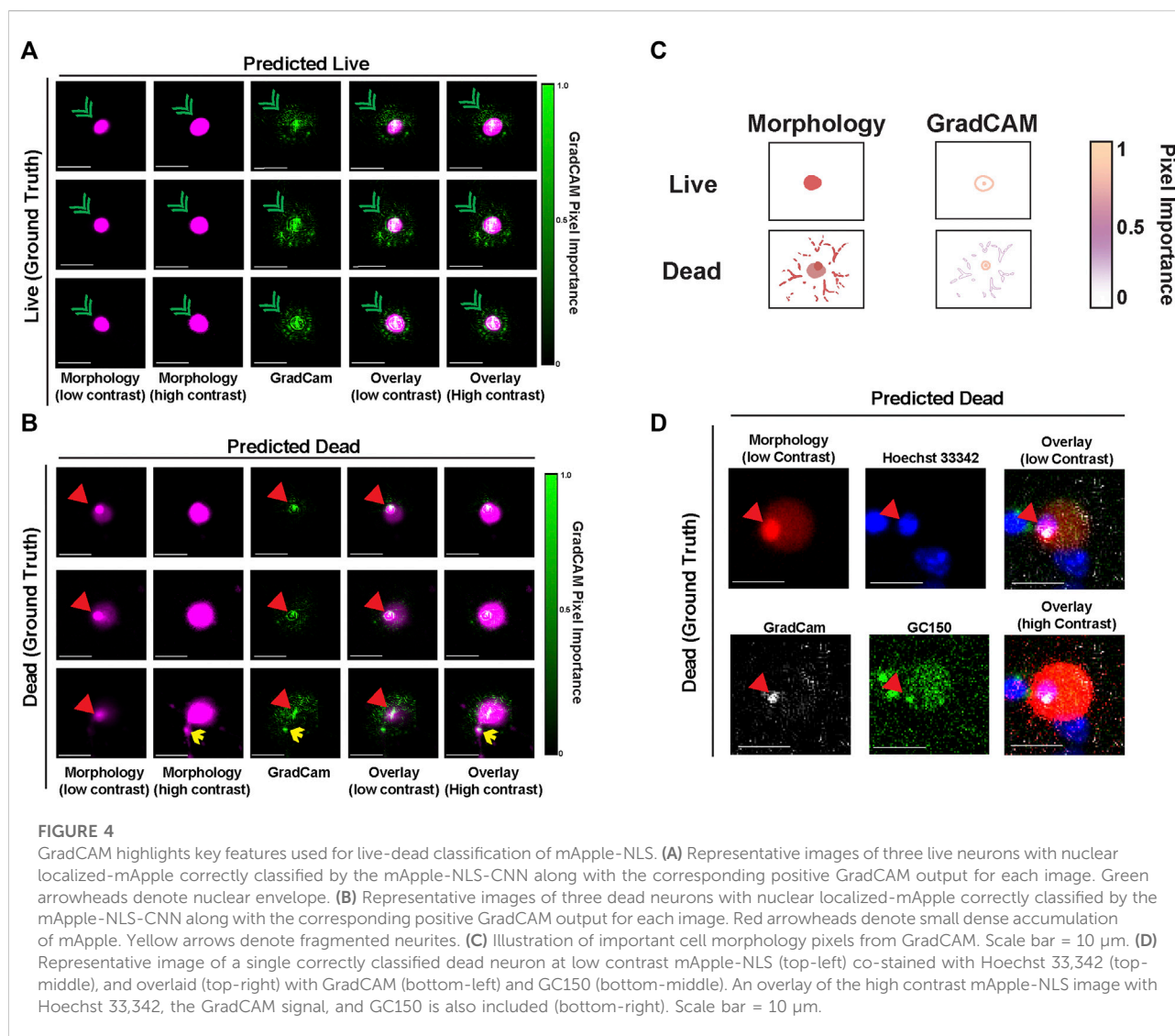
Accurate detection of neuronal death is important for assessing neurotoxicity. Using GEDI biosensors, we trained two novel CNNs, mApple-CNN and mApple-NLS-CNN, that detect cell death with superhuman accuracy by identifying morphological features related to cell death, despite receiving no explicit supervision to focus on those features. Using the



interpretative artificial intelligence technique GradCAM on mApple-NLS-CNN, we identified an accumulation of nuclear mApple signal associated with death that has not previously described. Our results demonstrate that nuclear-localized fluorescent protein signal can be used as a readout for neuronal death, enabling highly sensitive single-cell analyses of nuclear signals at large scales.

The use of a nuclear-localized signal holds several advantages over cell morphology for live imaging. First, in dense tissue, segmentation of individual nuclei can be easier than that of individual cells, because the cytoplasm of each cell spatially separates one nucleus from another. Second, most cell tracking algorithms operate on temporal-spatial separation between cells, and the extra spatial separation helps maintain

separation of cell tracks (Ulman et al., 2017). Third, in contrast to neurons, which are irregularly and variably shaped and show incredible diversity in the number and size of neurite projections, nuclei all have an oval shape and are consistent in size, making them more amenable to automated segmentation. Fourth, nuclear-localized signals are more flexible than cytoplasmic markers for multiplexing with other biosensors to probe for phenotypes of interest. However, nuclear-localized fluorescent protein has not previously been used as an indicator of cell death and toxicity. Indeed, we find that when neurons degenerate, changes in their overall morphology, such as neurite retraction and fragmentation and rounding of the soma, are easy to spot, whereas changes in nuclear-localized fluorescent protein are arguably more subtle (Figures 1D,E). Nevertheless, our data



indicate that key features—including an increase in area, the leaking of nuclear fluorescence into neurites, and the appearance of small dense accumulations—are equally strong indicators of death compared to neuronal morphology. Furthermore, with the availability of neural networks such as mApple-NLS-CNN to boost the scale and speed of image analysis, the use of nuclear morphology for detection of toxicity could be easily incorporated into experimental design.

Membrane permeant dyes that bind DNA like Hoechst 33,342 are often used as nuclear morphology markers for live cell imaging and have also been used as an indication of apoptotic cell death (Crowley et al., 2016). However, there are several practical advantages to the use of GC150-P2a-mApple-NLS or mApple-NLS-CNN over Hoechst 33,342 for tracking live cells in culture. First, Hoechst 33,342 stains all cell nuclei in cultures, while GC150-P2a-mApple-NLS or mApple-NLS alone can be specifically targeted to express in cell types of interest such as

with a neuron-specific promoter (hSyn1) used in this manuscript, facilitating a readout of cell death from specific cell types within a mixed culture. Second, Hoechst 33,342 only qualitatively distinguishes apoptotic cells from live cells due to the altered appearance of condensed DNA in apoptotic cells (Supplementary Figure S2) (Crowley et al., 2016). In contrast, the ratio-metric readout from GC150-P2a-mApple-NLS or the binary classification provided by the mApple-NLS-CNN model output provide quantitative readouts of death for each cell. Finally, some healthy cells undergoing mitosis may also have condensed DNA (Errami et al., 2013) and some cells can die by apoptosis in the absence of nuclear fragmentation (Zhang et al., 2001), making the Hoechst 33,342 signal difficult to use as an indicator of death in some instances. Thus, GC150-P2a-mApple-NLS and mApple-NLS-CNN have distinct advantages over the use of Hoechst 33,342 stain for reporting cell death in live cell imaging.

One surprising finding in this study was the appearance of small dense accumulation of mApple that appears after neuronal death (Figures 1E, 4B–D–4D; Supplementary Figure S1). Because this accumulation occurs within a backdrop of diffuse nuclear mApple-NLS fluorescence, it is difficult to see by eye without changing the contrast on the image. As this accumulation appears to co-localize with condensation of DNA that occurs during apoptosis (Toné et al., 2007), it is likely that this finding reflects a shrinking of the nuclear envelope around the condensed DNA, which concentrates mApple protein that cannot escape the nuclear envelope during death. In previous work, we found that the GEDI-CNN identified a signal within the nuclear region of the morphology signal that contributed to its superhuman accuracy at live/dead classification (Kim et al., 2014), and we speculate that the dense accumulation of mApple-NLS observed in this study and GEDI-CNN's recognition of patterns of free EGFP within the nucleus in our prior study represent the same phenomenon. However, the GEDI-CNN failed to translate to the mApple-NLS signal (Figure 1H), indicating that the nuclear signals detected in EGFP- and mApple-NLS transfected cells may be distinct. On the other hand, the size of nuclear-localized mApple signal has a different scale than non-targeted mApple or EGFP morphology signal (Figures 1F,G), and neural networks are scale-invariant, so the size difference alone may limit the ability to translate the GEDI-CNN from EGFP morphology signal to mApple-NLS signal (Han et al., 2020). Either way, this phenomenon within nuclear-localized fluorescence represents a new and robust feature of death and toxicity in neuronal cultures, and in combination with mApple-NLS-CNN it may enable new discoveries and therapeutic approaches to combat neurodegenerative disease.

Data availability statement

The raw data supporting the conclusion of this article will be made available by the authors, without undue reservation.

Ethics statement

The animal study was reviewed and approved by the Institutional Animal Care Use Committee (IACUC) of the University of California, San Francisco (UCSF).

Author contributions

JWL, SW, DL, and SF wrote the manuscript and conceptualized the manuscript. Data analysis and statistics by JWL, SW, DL, and JL. Robotic microscopy, transfections, and cell culture performed by SW. GEDI-CNN code base developed by DL and JWL. GEDI-CNN training and GradCAM visualizations

performed by DL. Custom Fiji scripts for analysis and curation of imaging experiments done by JWL and JL. All authors reviewed the manuscript.

Funding

This work was supported by the Koret Foundation Artificial Intelligence Program for Biomedical Research, the Taube/Koret Center for Neurodegenerative Disease, and grants from the NIH (U54 NS191046, R37 NS101996, RF1 AG058476, RF1 AG056151, RF1 AG058447, P01 AG054407, U01 MH115747, and R01 LM013617), AnswerALS and the Target ALS Foundation, the Amyotrophic Lateral Sclerosis Association Neuro Collaborative, a gift from Mike Frumkin, and the Department of Defense award W81XWH-13-ALSRP-TIA. Gladstone Institutes received support from a National Center for Research Resources Grant RR18928.

Acknowledgments

Kathryn Claiborn and Françoise Chanut provided editorial assistance, Kelley Nelson and Gayane Abramova provided administrative assistance. Neha Arora and Daniela Melandri contributed to image curation. We thank the NVIDIA Corporation for the donation of the Titan Xp and Quadro P6000 GPUs used for this research.

Conflict of interest

The authors declare that the research was conducted in the absence of any commercial or financial relationships that could be construed as a potential conflict of interest.

Publisher's note

All claims expressed in this article are solely those of the authors and do not necessarily represent those of their affiliated organizations, or those of the publisher, the editors and the reviewers. Any product that may be evaluated in this article, or claim that may be made by its manufacturer, is not guaranteed or endorsed by the publisher.

Supplementary material

The Supplementary Material for this article can be found online at: <https://www.frontiersin.org/articles/10.3389/ftox.2022.935438/full#supplementary-material>

SUPPLEMENTARY FIGURE S1

Representative examples of death in cells expressing mApple-NLS. High and low contrast images of six dead neurons demonstrating the small dense accumulation of mApple (red arrows) and the presence of neurites (green asterisks).

SUPPLEMENTARY FIGURE S2

Representative examples of live and dead cells stained with Hoechst 33342. **(A)** Live cell expressing hSyn1-GC150-NLS-P2A-mApple-NLS stained with Hoechst 33342. White arrow indicates Hoechst 33342 staining pattern. **(B)** Dead cell expressing hSyn1-GC150-NLS-P2A-mApple-NLS stained with Hoechst 33342. White arrow

indicates Hoechst 33342 staining pattern. Yellow arrow indicates dense accumulation of mApple. Scale bar = 10 μ m.

SUPPLEMENTARY MOVIE S1

Timelapse movie of morphological and GC150 changes associated with neuronal death. Timelapse movie of overlaid GC150-NLS and mApple-NLS channels (top), low contrast mApple-NLS channel alone (middle), and high contrast mApple-NLS channel (bottom) showing the onset of GC150-NLS signal and corresponding dense accumulation of mApple and appearance of neurites. Images were taken every 8 h. Scale bar = 10 μ m.

References

- Alladin, A., Chaible, L., Garcia Del Valle, L., Sabine, R., Loeschinger, M., Wachsmuth, M., et al. (2020). Tracking cells in epithelial acini by light sheet microscopy reveals proximity effects in breast cancer initiation. *Elife* 9, e54066. doi:10.7554/eLife.54066
- Cooper, D. J., Zunino, G., Bixby, J. L., and Lemmon, V. P. (2017). Phenotypic screening with primary neurons to identify drug targets for regeneration and degeneration. *Mol. Cell. Neurosci.* 80, 161–169. doi:10.1016/j.mcn.2016.07.001
- Crowley, L. C., Marfell, B. J., and Waterhouse, N. J. (2016). Analyzing cell death by nuclear staining with Hoechst 33342. *Cold Spring Harb. Protoc.* 2016 (9), pdb.prot087205. doi:10.1101/pdb.prot087205
- Errami, Y., Naura, A. S., Kim, H., Ju, J., Suzuki, Y., El-Bahrawy, A. H., et al. (2013). Apoptotic DNA fragmentation may be a cooperative activity between caspase-activated deoxyribonuclease and the poly(ADP-ribose) polymerase-regulated DNAIL3, an endoplasmic reticulum-localized endonuclease that translocates to the nucleus during apoptosis. *J. Biol. Chem.* 288 (5), 3460–3468. doi:10.1074/jbc.M112.423061
- Galluzzi, L., Aaronson, S. A., Abrams, J., Alnemri, E. S., Andrews, D. W., Baehrecke, E. H., et al. (2009). Guidelines for the use and interpretation of assays for monitoring cell death in higher eukaryotes. *Cell. Death Differ.* 16 (8), 1093–1107. doi:10.1038/cdd.2009.44
- Galluzzi, L., Vitale, I., Aaronson, S. A., Abrams, J. M., Adam, D., Agostinis, P., et al. (2018). Molecular mechanisms of cell death: Recommendations of the nomenclature committee on cell death 2018. *Cell. Death Differ.* 25 (3), 486–541. doi:10.1038/s41418-017-0012-4
- Hadjantonakis, A. K., and Papaioannou, V. E. (2004). Dynamic *in vivo* imaging and cell tracking using a histone fluorescent protein fusion in mice. *BMC Biotechnol.* 4, 33. doi:10.1186/1472-6750-4-33
- Han, Y., Roig, G., Geiger, G., and Poggio, T. (2020). Scale and translation-invariance for novel objects in human vision. *Sci. Rep.* 10 (1), 1411. doi:10.1038/s41598-019-57261-6
- He, K., Zhang, X., Ren, S., and Sun, J. (2015). Deep residual learning for image recognition. Available: <https://ui.adsabs.harvard.edu/abs/2015arXiv151203385H> (Accessed December 01, 2015).
- Hou, L., Liu, K., Li, Y., Ma, S., Ji, X., and Liu, L. (2016). Necrotic pyknosis is a morphologically and biochemically distinct event from apoptotic pyknosis. *J. Cell. Sci.* 129 (16), 3084–3090. doi:10.1242/jcs.184374
- Hughes, A. J., Mornin, J. D., Biswas, S. K., Beck, L. E., Bauer, D. P., Raj, A., et al. (2018). Quanti.us: A tool for rapid, flexible, crowd-based annotation of images. *Nat. Methods* 15 (8), 587–590. doi:10.1038/s41592-018-0069-0
- Kepp, O., Galluzzi, L., Lipinski, M., Yuan, J., and Kroemer, G. (2011). Cell death assays for drug discovery. *Nat. Rev. Drug Discov.* 10 (3), 221–237. doi:10.1038/nrd3373
- Kim, C. K., Miri, A., Leung, L. C., Berndt, A., Mourrain, P., Tank, D. W., et al. (2014). Prolonged, brain-wide expression of nuclear-localized GCaMP3 for functional circuit mapping. *Front. Neural Circuits* 8, 138. doi:10.3389/fnirc.2014.00138
- Kingma, D. P., and Ba, J. (2014). Adam: A method for stochastic optimization. Available: <https://ui.adsabs.harvard.edu/abs/2014arXiv1412.6980K> (Accessed December 01, 2014).
- Lewerenz, J., and Maher, P. (2015). Chronic glutamate toxicity in neurodegenerative diseases—what is the evidence? *Front. Neurosci.* 9, 469. doi:10.3389/fnins.2015.00469
- Linsley, J. W., Linsley, D. A., Lamstein, J., Ryan, G., Shah, K., Castello, N. A., et al. (2021). Superhuman cell death detection with biomarker-optimized neural networks. *Sci. Adv.* 7 (50), eabf8142. doi:10.1126/sciadv.abf8142
- Linsley, J. W., Reisine, T., and Finkbeiner, S. (2019). Cell death assays for neurodegenerative disease drug discovery. *Expert Opin. Drug Discov.* 14 (9), 901–913. doi:10.1080/17460441.2019.1623784
- Linsley, J. W., Shah, K., Castello, N., Chan, M., Haddad, D., Doric, Z., et al. (2021). Genetically encoded cell-death indicators (GEDi) to detect an early irreversible commitment to neurodegeneration. *Nat. Commun.* 12 (1), 5284. doi:10.1038/s41467-021-25549-9
- Linsley, J. W., Tripathi, A., Epstein, I., Schmunk, G., Mount, E., Campioni, M., et al. (2019). Automated four-dimensional long term imaging enables single cell tracking within organotypic brain slices to study neurodevelopment and degeneration. *Commun. Biol.* 2, 155. doi:10.1038/s42003-019-0411-9
- Selvaraju, R. R., Cogswell, M., Das, A., Vedantam, R., Parikh, D., and Batra, D. (2016). Grad-CAM: Visual explanations from deep networks via gradient-based localization. Available: <https://ui.adsabs.harvard.edu/abs/2016arXiv161002391S> (Accessed December 01, 2014).
- Sherman, S. P., and Bang, A. G. (2018). High-throughput screen for compounds that modulate neurite growth of human induced pluripotent stem cell-derived neurons. *Dis. Model. Mech.* 11 (2), dmm031906. doi:10.1242/dmm.031906
- Skibinski, G., Hwang, V., Ando, D. M., Daub, A., Lee, A. K., Ravisankar, A., et al. (2017). Nrf2 mitigates LRRK2- and alpha-synuclein-induced neurodegeneration by modulating proteostasis. *Proc. Natl. Acad. Sci. U. S. A.* 114 (5), 1165–1170. doi:10.1073/pnas.1522872114
- Sullivan, D. P., Winsnes, C. F., Åkesson, L., Hjelmare, M., Wiking, M., Schutten, R., et al. (2018). Deep learning is combined with massive-scale citizen science to improve large-scale image classification. *Nat. Biotechnol.* 36 (9), 820–828. doi:10.1038/nbt.4225
- Tomer, R., Lovett-Barron, M., Kauvar, I., Andalman, A., Burns, V. M., Sankaran, S., et al. (2015). SPED light sheet microscopy: Fast mapping of biological system structure and function. *Cell.* 163 (7), 1796–1806. doi:10.1016/j.cell.2015.11.061
- Toné, S., Sugimoto, K., Tanda, K., Suda, T., Uehira, K., Kanouchi, H., et al. (2007). Three distinct stages of apoptotic nuclear condensation revealed by time-lapse imaging, biochemical and electron microscopy analysis of cell-free apoptosis. *Exp. Cell. Res.* 313 (16), 3635–3644. doi:10.1016/j.yexcr.2007.06.018
- Ulman, V., Maska, M., Magnusson, K. E. G., Ronneberger, O., Haubold, C., Harder, N., et al. (2017). An objective comparison of cell-tracking algorithms. *Nat. Methods* 14 (12), 1141–1152. doi:10.1038/nmeth.4473
- Zhang, M., Li, Y., Zhang, H., and Xue, S. (2001). BAPTA blocks DNA fragmentation and chromatin condensation downstream of caspase-3 and DFF activation in HT-induced apoptosis in HL-60 cells. *Apoptosis.* 6 (4), 291–297. doi:10.1023/a:1011387509290
- Zhou, Y., and Danbolt, N. C. (2014). Glutamate as a neurotransmitter in the healthy brain. *J. Neural Transm.* 121 (8), 799–817. doi:10.1007/s00702-014-1180-8